ACS APPLIED MATERIALS & INTERFACES

Research Article

www.acsami.org

Stepwise-Acid-Active Multifunctional Mesoporous Silica Nanoparticles for Tumor-Specific Nucleus-Targeted Drug Delivery

Ze-Yong Li,‡ Yun Liu,‡ Jing-Jing Hu, Qi Xu, Li-Han Liu, Hui-Zhen Jia, Wei-Hai Chen, Qi Lei, Lei Rong, and Xian-Zheng Zhang*

Key Laboratory of Biomedical Polymers of the Ministry of Education & Department of Chemistry, Wuhan University, Wuhan 430072, P. R. China

Supporting Information

ABSTRACT: In this paper, a novel stepwise-acid-active multifunctional mesoporous silica nanoparticle (MSN-^{SA}TAT&^{DMA}K$_{11}$) was developed as a drug carrier. The MSN-^{SA}TAT&^{DMA}K$_{11}$ is able to reverse its surface charge from negative to positive in the mildly acidic tumor extracellular environment. Then, the fast endo/lysosomal escape and subsequent nucleus targeting as well as intranuclear drug release can be realized after cellular internalization. Because of the difference in acidity between the tumor extracellular environment and that of endo/lysosomes, this multifunctional MSN-^{SA}TAT&^{DMA}K$_{11}$ exhibits a stepwise-acid-active drug delivery with a tumor-specific nucleus-targeted property.

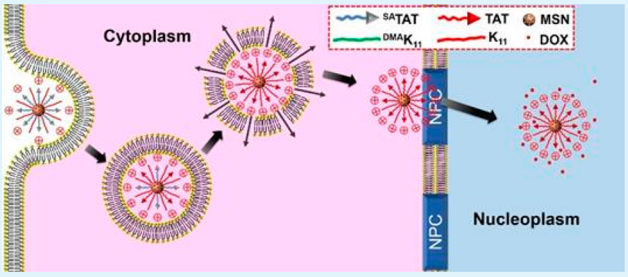

KEYWORDS: *mesoporous silica nanoparticle, drug release, stepwise-acid-activation, tumor-specificity, nucleus-targeting*

INTRODUCTION

An important advancement in cancer therapy is to develop personalized and tailored agents with exclusive selectivity for killing tumor cells without any unwanted bystander effects of the magic bullet concept.[1] Developments in antitumor drug and gene therapies suggest that this concept is not a pipe dream, and a tumor-specific drug delivery may prove possible to achieve to some extent. Researchers aim to deliver antitumor drugs to tumor cells specifically without affecting normal cells and to subsequently deliver them to hypersensitive subcellular sites within the tumor cells.[2] In this regard, the nucleus is usually regarded as the final target where the genetic material works. Meanwhile, the antitumor efficacy would be enhanced profoundly by the efficient intranuclear import of DNA-damaging drugs, such as doxorubicin (DOX). Intensive efforts have been made in the construction of smart nanosized drug delivery systems (DDSs) for controlled release based on mesoporous silica nanoparticles (MSNs)[3,4] due to their high specific surface areas, large pore volumes, facile postsynthesis and bioconjugation, good biocompatibility, and bio- and physicochemical stability.[5−7]

Tumor-specific nucleus-targeted delivery is a critical challenge since the nanocarrier should satisfy the following requirements: (i) it should be tumor specific, that is, selectively deliver cargoes to the targeted tumors without any harmful side effects;[8] (ii) it should be capable of endo/lysosomal escape to avoid the degradation of internalized nanocarriers and cargoes;[9] (iii) it should target the nucleus to achieve the intranuclear localization of cargoes;[10] and (iv) it should be small enough for nuclear import.[6,11,12] To address the challenge of tumor specificity, tumor environment[13,14] responsive delivery systems were developed to realize tumor targeting via the extracellular activation of nanocarriers in recent years.[15−17] Among the tumor extracellular stimuli, pH is the most frequently used one since the acidity in different sites and cellular compartments varies tremendously. The tumor extracellular compartments are more acidic (pH 5.8−7.1)[18] than those in normal tissues (pH 7.4), while the endo/lysosomal pH is even lower (pH 5.0−5.5).[19] Additionally, to achieve "stealth" manners during circulation and before arriving at the target site, tumor-acidity-activated charge-conversional featured nanocarriers were developed for enhanced tumor-specific cellular uptake.[15,20,21] Such nanocarriers maintain a negative charge during circulation[15,22] with a prolonged circulation time[23,24] and then become positively charged upon their arrival at the target tumor tissue to be readily endocytosed by the tumor cells.[15,20]

The second important issue that needs to be addressed is the endo/lysosomal escape for the endocytosed carriers. Several strategies were proposed, including pH-induced charge conversion,[22,25] pH-stimulated membrane fusion and disruption,[26−28] pH-induced swelling,[29,30] and the introduction of chemical ligands for endo/lysosomal escape.[31,32] Moreover, it is vitally important for the internalized nanocarriers to be liberated into the cytosol and then imported to target the nucleus with the facilitation of a nuclear localization signal (NLS). As one of the most important NLS peptides, the TAT peptide exhibits fast endo/lysosomal escape,[33] quick nuclear localization, and subsequent recognition by nuclear pore

Received: June 18, 2014
Accepted: August 8, 2014
Published: August 8, 2014

complexes (NPCs).[34−36] However, the TAT peptide tends to interact with serum components, which causes its rapid clearance from circulation because of the inherent cationic nature. To overcome this, TAT was succinyl-amidized to prepare ^{SA}TAT with the inhibition of nonspecific interaction, which can be regenerated in endo/lysosomes for nucleus-targeted drug delivery.[37]

Here, we report on a delicately designed MSN-based MSN-^{SA}TAT&$^{DMA}K_{11}$ as a novel stepwise pH-responsive drug carrier. The MSN-^{SA}TAT&$^{DMA}K_{11}$ can respond to tumor extracellular and endo/lysosomal pH gradients with different acid sensitivities. It is expected that the stepwise pH-responsive behavior of the carrier will promote cell internalization at the tumor tissue via tumor-acidity-activated charge conversion and will facilitate the fast endo/lysosomal escape as well as the subsequent nucleus targeting via endo/lysosome-acidity-activated charge conversion (Scheme 1).

Scheme 1. Schematic Illustration of the Smart Nanocarrier (DOX@MSN-^{SA}TAT&$^{DMA}K_{11}$) with Stepwise pH Response to the Tumor Extracellular Matrix and Intracellular Compartments for Tumor-Specific Nucleus-Targeted Drug Delivery

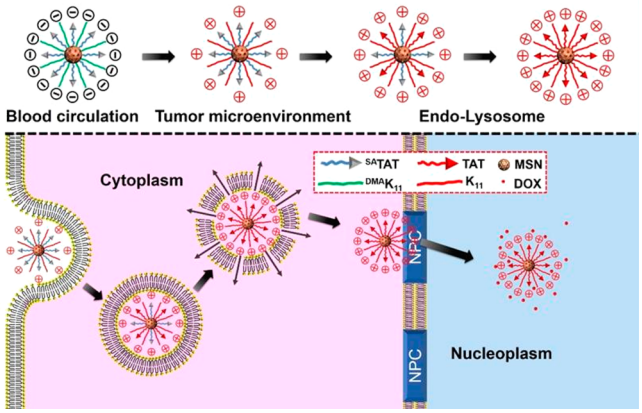

EXPERIMENTAL SECTION

Materials. *N*-Cetyltrimethylammonium bromide (CTAB) and tetraethylorthosilicate (TEOS) were obtained from Shanghai Reagent Chemical Co. (China) and used as received. Doxorubicin hydrochloride (DOX) was purchased from Zhejiang Hisun Pharmaceutical Co. (China). Tris(3-hydroxypropyltriazolylmethyl)amine (THPTA) was synthesized in our lab.[38] Dimethylmaleic anhydride (DMA) and succinic anhydride (SA) were purchased from Aladdin Reagent Co. Ltd. (Shanghai, China). Dulbecco's Modified Eagle Medium (DMEM), fetal bovine serum (FBS), 3-[4,5-dimethylthiazol-2-yl]-2,5-diphenyltetrazolium-bromide (MTT), Hochest 33342, Lysotracker Red DND-99, and wheat germ agglutinin (WGA) Alexa Fluor 594 conjugate were purchased from Invitrogen Co. (United States). All of the other reagents and solvents were provided by Shanghai Reagent Chemical Co. (China) and used without any further treatment or purification. The standard formulas were used to prepare D-Hank's solution (0.40 g of KCl, 0.06 g of KH_2PO_4, 0.35 g of $NaHCO_3$, 0.048 g of Na_2HPO_4, 8.00 g of NaCl, 1 L H_2O), lysis solution A (100 mM NaCl solution with 1 mM EDTA, 1% Triton X-100, and 10 mM Tris buffer (pH 7.4)), and lysis solution B (0.5% Triton X-100, 1 M NaOH).

Methods. An AVATAR 360 spectrometer was used for Fourier transform infrared (FT-IR) spectra recording. A TGS-2 thermogravimetric analyzer (PerkinElmer) was used for the performance of thermal gravimetric analysis (TGA). A RF-5301PC spectrofluorophotometer (Shimadzu) was used to record fluorescence spectra. Transmission electron microscopy (TEM) experiments were carried out on a JEM-2100 instrument operating at 200 kV. Surface area was calculated by the Brunauer−Emmett−Teller (BET) method, and the pore size distributions were obtained by the Barrett−Joyner−Halenda (BJH) approach (ASAP2020, micromeritics).

Preparation of MSN. The applied MSN was synthesized according to the literature with some modification.[39] As a typical procedure, hexadecyl trimethylammonium chloride (CTAC, 2.6 g) and a triblock copolymer (Pluronic F127, 2.0 g) were dissolved in a hydrochloric acid solution (30 g, pH 0.5) at room temperature as the cationic and nonionic surfactants, respectively. Tetraethyl orthosilicate (TEOS, 3.5 g) then was added to the mixture. The mixture became clear with vigorous stirring. After being stirred for 24 h, the clear mixture was turned into a white gel via the addition of ammonium hydroxide (14.7 M, 3.0 g). After being aged at room temperature for 24 h, the gel was dried at 60 °C overnight. To remove the surfactants, the white solid was refluxed for 24 h in a solution of 5.0 mL of HCl (37%) and 200.0 mL of 1% NaCl containing methanol, washed thoroughly with ethanol, and redispersed in ethanol.

Preparation of Amino-Functionalized MSN (MSN-NH_2) and Fluorescence-Labeled Amino-Functionalized MSN (FITC-MSN-NH_2). The MSN (200 mg) in ethanol (20 mL) was functionalized with 1 mL of 3-aminopropyltriethoxysilane (APTES) under reflux condition for 12 h to produce MSN-NH_2 nanoparticles. After centrifugation and being washed with ethanol, the nanoparticles were redispersed in 20 mL of ethanol. FITC-MSN-NH_2 was simply prepared by the reaction of MSN (200 mg) with FITC-APTES (containing excessive APTES); thereinto, FITC-APTES was obtained by the reaction between FITC (5 mg) and APTES (1 mL) at room temperature in the dark and a N_2 atmosphere over 6 h.

Preparation of MSN-alkyne and FITC-MSN-alkyne. The MSN-NH_2 (100 mg) in methanol (20 mL) was reacted with 2 mL of propargyl bromide for 24 h. The nanoparticles were separated by centrifugation and washed extensively with ethanol. A similar procedure was adopted to produce FITC-MSN-alkyne.

Synthesis of Amidized Azidopeptides. Two azidopeptides (N_3-K_{11}: N_3-GKKKKKKKKKK-NH_2; N_3-TAT: N_3-GYGRKKRRQRRR-NH_2) were synthesized manually employing a standard Fmoc chemistry that used 6 equiv of Fmoc-amino acid or azidobenzoic acid as well as HATU (1-[bis(dimethylamino)methylene]-1*H*-1,2,3-triazolo[4,5-*b*]pyridinium 3-oxid hexafluorophosphate) and NMM (*N*-methylmorpholine) as coupling reagents in each step. Finally, the total cleavage was done (82.5% trifluoroacetic acid, 7.5% phenol, 2.5% 1,2-ethanedithiol, 5% thioanisole, 2.5% distilled (DI) water; 2.0 h), followed by the precipitation of the peptide in cold ether.

N_3-TAT (20 mg) was dissolved in 2 mL of anhydrous DMF. Excessive SA (20 mg) and 2,6-lutidine (20 mg) were added to the solution and it was stirred for 1 h. After precipitation, the crude product was collected and dialyzed against pH 7.4 phosphate-buffered saline (PBS) (MWCO 1000), followed by lyophilization. The product, amidized N_3-TAT (N_3-^{SA}TAT), was analyzed by high-performance liquid chromatography (HPLC) and electrospray ionization mass spectrometry (ESI-MS).

N_3-K_{11} (20 mg) was dissolved in DI water, and the solution pH was adjusted to 8−9. Excessive DMA (100 mg) was added to the solution, and the pH was kept in the range of 8−9 using 1 M NaOH during the reaction. The reaction was allowed to continue at room temperature overnight after the pH was constant. The product (N_3-$^{DMA}K_{11}$) was obtained after being dialyzed against water at pH 8.5 and freeze-dried.

Preparation of MSN-^{SA}TAT&$^{DMA}K_{11}$ and FITC-MSN-^{SA}TAT&$^{DMA}K_{11}$. MSN-alkyne (15 mg), N_3-^{SA}TAT (10 mg), N_3-K_{11} (10 mg), CuBr (5 mg), and THPTA (10 mg) were suspended in 6 mL of dimethylformamide (DMF) under N_2 condition. After being stirred for 2 d at room temperature, the resulting nanoparticles (MSN-^{SA}TAT&K_{11}) were purified by centrifugation and washed several times with ethylenediaminetetraacetic acid (EDTA) dissolved in 7.4 PBS. Finally, MSN-^{SA}TAT&$^{DMA}K_{11}$ nanoparticles were obtained via the DMA amidization of MSN-^{SA}TAT&K_{11} and stored under liquid

nitrogen. FITC-MSN-^{SA}TAT&^{DMA}K$_{11}$ nanoparticles were simply obtained by using FITC-MSN-alkyne in the "click reaction".

Preparation of DOX@MSN-^{SA}TAT&^{DMA}K$_{11}$. MSN-^{SA}TAT&^{DMA}K$_{11}$ (10 mg) and DOX (5 mg) were suspended in 5 mL of anhydrous DMF and stirred at 4 °C for 24 h. The free DOX was removed by washing with ice-cold 7.4 PBS.

Protein Adsorption. To investigate the pH effect on protein adsorption on different nanoparticles, the MSN-TAT&^{DMA}K$_{11}$, MSN-^{SA}TAT&^{DMA}K$_{11}$, and MSN-^{SA}TAT&^{SA}K$_{11}$ nanoparticles were respectively incubated with human serum albumin (HSA) solution in PBS (50 mM) of pH 6.8 or 7.4 with the final concentration of nanoparticles and HSA being 0.10 and 0.15 mg mL^{-1}. After the nanoparticles were incubated at 37 °C for the indicated time, samples were withdrawn after vigorous stirring and centrifuging at 12 000 rpm for 10 min. The HSA concentration of the supernatant was quantified using a UV−vis spectrometer by measuring the maximal absorbance (λ = 280 nm). Then, the adsorbed HSA on the nanoparticles was calculated according to the report.[40]

pH-Induced Charge Conversion of Nanoparticles. The nanoparticles were dispersed in buffer solutions (50 mM) of pH values 7.4, 6.8, or 5.0 at the concentration of 0.1 mg mL^{-1}. The samples were immersed and shaken in a water bath at 37 °C. The samples were withdrawn at timed intervals, and their ζ-potentials were determined using the Zeta-Nanosizer.

In Vitro Cytotoxicity. HeLa cells were seeded on a 96-well dish with 200 μL DMEM containing 10% FBS. After incubation (37 °C and 5% CO_2) for 24 h, the original culture media in each well was replaced with 200 μL fresh DMEM containing the MSN-^{SA}TAT&^{DMA}K$_{11}$, MSN-^{DMA}K$_{11}$, DOX@MSN-^{SA}TAT&^{DMA}K$_{11}$, or DOX@MSN-^{DMA}K$_{11}$ nanoparticles at the indicated nanoparticle or DOX concentrations. The incubation continued for 48 h. Next, the media were replaced with fresh DMEM and MTT stock solution (20 μL, 5 mg mL^{-1} in PBS). After incubation for another 4 h, the MTT medium was removed and 200 μL dimethyl sulfoxide (DMSO) was added to the wells, and the dish was shaken at room temperature. The optical density (OD) was measured, and the viability was calculated.

In Vitro Release Studies. The release experiments were performed at pH values of 7.4, 6.8, and 5.0. For each release study, 1 mg of DOX@MSN-^{SA}TAT&^{DMA}K$_{11}$ nanoparticles were suspended in 1 mL PBS (pH 7.4), and the suspension was put into a dialysis tube that was directly immersed into 10 mL of buffer solution with the indicated pH and shaken in a water bath at 37 °C. The concentrations of the released DOX were calculated by measuring their fluorescence intensity (λ_{ex} = 488 nm, λ_{em} = 560 nm) with reference to the standard curve. After each measurement, the external buffer solution of the dialysis tube was refreshed immediately.

Confocal Laser Scanning Microscopy (CLSM). HeLa cells were plated onto glass-bottom Petri dishes (35 mm × 10 mm). After incubation in a humidified 5% CO_2 atmosphere for 24 h, the cells were treated with 1 mL of FITC-MSN-^{SA}TAT&^{DMA}K$_{11}$ or FITC-MSN-^{DMA}K$_{11}$ nanoparticles at the same final concentration of 10 μg mL^{-1} in fresh DMEM at pH 7.4 or 6.8, respectively. After incubation in the dark for different time periods (2, 4, 8, and 24 h), the cell nuclei were stained with Hoechst 33342, the acidic organelles were selectively stained with Lysotracker Red DND-99, and the plasma membranes were selectively stained with WGA Alexa Fluor 594 conjugate prior to imaging under a confocal laser scanning microscope (NOL-LSM 710 or Nikon C1-si).

Cellular Uptake Measured by Flow Cytometry. HeLa cells were seeded onto 6-well plates in 1 mL of DMEM medium and allowed to grow for 24 h. The media were replaced with FITC-MSN-^{SA}TAT&^{DMA}K$_{11}$ or FITC-MSN-^{SA}TAT&^{SA}K$_{11}$ containing DMEM of pH 7.4 or 6.8, respectively. After incubation for 2 h at 37 °C, the cells were washed with PBS and digested by trypsin. The trypsinized cells were harvested and suspended in PBS, and they were then centrifuged at 1000 rpm for 3 min at 4 °C. The supernatants were removed, and the cell pellets were washed with cold PBS three times to remove the residual nanoparticles. After that, each sample was quickly analyzed on a flow cytometer (BD FACSAria TM III, USA).

Cell Image by Bio-TEM. The MSN-^{SA}TAT&^{DMA}K$_{11}$ or MSN-^{DMA}K$_{11}$ (50 μg mL^{-1}) treated cells were fixed with glutaraldehyde in PBS overnight at 4 °C. After being rinsed three times in 0.1 M cacodylate buffer, the samples were postfixated with a 2% osmiumtetroxide (OsO_4) solution for 1 h at 4 °C. Then they were dehydrated in a graded ethanol series of 30%, 50%, 70%, and 90%. Subsequently, the samples were placed in resin plates and polymerized at 60 °C for 8 h. Ultrathin (~70 nm) sections were cut with a sliding ultramicrotome and then loaded on the copper grids and observed with the FEI Tecani G20 TWIN.

Nuclear Quantification of Silicon and DOX.[6] HeLa cells were seeded onto 6-well plates and cultured in DMEM with 10% FBS. After a 24 h incubation, the cells were incubated with MSN-^{SA}TAT&^{DMA}K$_{11}$ or MSN-^{DMA}K$_{11}$ nanoparticles (50 μg mL^{-1}) for 24 h. The cells were washed three times with D-Hank's solution and then were trypsinized. After being centrifuged and washed twice with D-Hank's solution, the cells were suspended in lysis solution A at 4 °C for 10 min to separate the cells nuclei from the cytosol. After centrifugation, the resulting precipitate was washed twice with D-Hank's solution, and cell nuclei were finally collected. Then lysis solution B was added to digest the nuclei with ultrasound. The mass of silicon from MSN-^{SA}TAT&^{DMA}K$_{11}$ or MSN-^{DMA}K$_{11}$ in the Hela cells nuclei was measured by atomic absorption spectroscopy (AAS). Similarly, the mass of DOX in the nuclei was measured by fluorescence spectrometry when HeLa cells were incubated with DOX@MSN-^{SA}TAT&^{DMA}K$_{11}$ or DOX@MSN-^{DMA}K$_{11}$ for 24 h.

RESULTS AND DISCUSSION

Preparation and Characterization of MSN-^{SA}TAT&^{DMA}K$_{11}$. The azidopeptides (N_3-TAT and N_3-K$_{11}$, see Schemes S1 and S2 of the Supporting Information for detailed structures) were manually synthesized according to the standard Fmoc solid-phase peptide synthesis (SPPS) protocol.[41] Next, the succinyl amidized N_3-TAT (N_3-^{SA}TAT) was prepared according to the literature.[37] Although the two lysine residue amines were amidized to obtain the succinyl amides, the glutamine amide and guanidinyl groups were not affected as determined by ESI-MS spectra (Figure S3B, Supporting Information).

As we know, a small particle size is the key factor for the intranuclear transport of the nanoparticles since the nuclear membrane is punctured by thousands of NPCs with diameters of 20−70 nm depending on the cell type and cycle.[12] Here, MSN was synthesized with a diameter of 20−50 nm (Figure 1A) according to the method reported by Imai et al.[39] The powder X-ray diffraction (XRD) pattern of MSN showed a typical hexagonal array with three low-angle reflections indexed as (100), (110), and (200) Bragg peaks (Figure S4, Supporting Information), which confirmed the well-ordered structures of the as-synthesized MSNs. Nitrogen adsorption and desorption isotherm characterization indicated that the MSNs possessed well-defined mesoporous apertures of around 2.6 nm and relatively high surface areas of 1166 m^2 g^{-1} (Figure 1C,D), which are in accordance with the TEM observations. It is worth noting that the large pores of around 18 nm were attributed to the interparticle space among the MSNs.

The surface of MSN was first functionalized with 3-aminopropyltriethoxysilane to obtain MSN-NH_2, which was then allowed to react with propargyl bromide to prepare MSN-alkyne. The FT-IR spectrum of MSN-alkyne showed an alkyne absorption band at 2130 cm^{-1} (Figure S5, Supporting Information), which indicated the successful functionalization. Next, both N_3-^{SA}TAT and N_3-K$_{11}$ obtained above were conjugated onto the outside surface of MSN-alkyne via "click chemistry" to prepare MSN-^{SA}TAT&K$_{11}$. Finally, the negatively

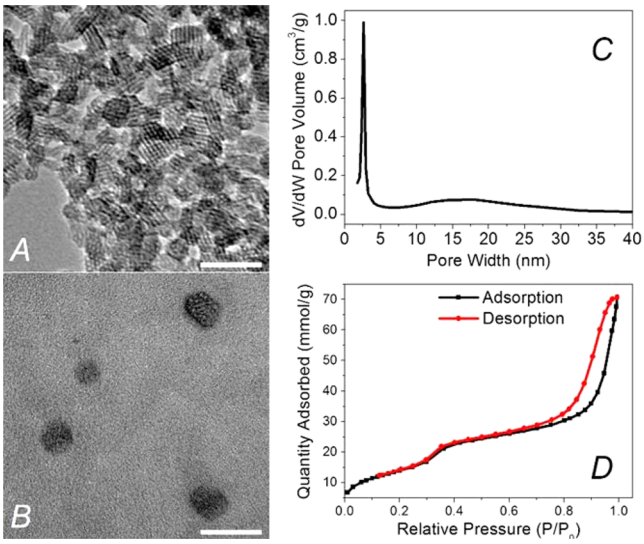

Figure 1. TEM images of MSN (A) and FITC-MSN-^{SA}TAT&^{DMA}K$_{11}$ (B). Barrett–Joyner–Halenda pore distribution (C) and nitrogen adsorption and desorption isotherms (D) of MSN. Scale bars: 50 nm.

charged MSN-^{SA}TAT&^{DMA}K$_{11}$ nanoparticles were prepared by the dimethylmaleic amidization of MSN-^{SA}TAT&K$_{11}$ (Scheme S3, Supporting Information). Its dynamic light scanning (DLS) diameter (*z*-average: ~78 nm, Figure S7A of the Supporting Information) was larger than its TEM diameter caused by hydrated layers. The typical absorption peaks of amide I and amide II band at 1650 and 1550 cm^{-1} (Figure S5, Supporting Information) and verified the conjugation of the peptide moiety. Thermal gravimetric analysis (TGA) was utilized to monitor the process of functionalization. As shown in the TGA curves in Figure S6 of the Supporting Information, the weight losses of MSN, MSN-alkyne, and MSN-^{SA}TAT&^{DMA}K$_{11}$ were 27.0%, 32.5%, and 47.0%, respectively, when the temperature was increased to 800 °C. The gradually increased weight loss indicated not only the alkyne moiety but also that the peptide component was incorporated. According to the TGA data, the mass percentage of conjugated peptides in MSN-^{SA}TAT&^{DMA}K$_{11}$ was calculated to be 21.5% based on the equation: (1−32.5%) × (1 − x) = 1−47%, where x is the weight percentage of the conjugated peptides in MSN-^{SA}TAT&^{DMA}K$_{11}$. Moreover, the fluorescence-labeled MSN-^{SA}TAT&^{DMA}K$_{11}$ (FITC-MSN-^{SA}TAT&^{DMA}K$_{11}$) was prepared by conjugating N$_3$-^{SA}TAT and N$_3$-K$_{11}$ onto the surface of the fluorescence-labeled MSN-alkyne (FITC-MSN-alkyne) via click chemistry followed by dimethylmaleic amidization. It was found that the negatively charged FITC-MSN-^{SA}TAT&^{DMA}K$_{11}$ showed excellent dispersibility (Figure 1B) attributed to the introduction of amidized peptides.

pH-Triggered Charge Conversion and Protein Adsorption. The key feature of MSN-^{SA}TAT&^{DMA}K$_{11}$ is to realize a stepwise pH response to the mildly acidic tumor microenvironment and the more acidic intracellular endo/lysosomes. To demonstrate its pH response to the tumor extracellular acidity, we measured the zeta potential of the MSN-^{SA}TAT&^{DMA}K$_{11}$ nanoparticles in buffer solutions at pH values of 7.4 and 6.8 to simulate the physiological environment and tumor microenvironment, respectively. The zeta potential of MSN-^{SA}TAT&^{DMA}K$_{11}$ increased significantly at pH 6.8. In detail, it changed rapidly from negative (−7.9 mV) to positive (+7.2 mV) within 2 h (Figure 2A) because of the hydrolysis of the lysyl dimethylmaleic amides in ^{DMA}K$_{11}$ under the simulated tumor extracellular matrix. In contrast, the zeta potential increased slowly from −14.1 to −7.7 mV at pH 7.4 within 2 h. We further measured the zeta potential of MSN-^{SA}TAT&^{DMA}K$_{11}$ in pH 5.0 acetate buffer solution (simulating the endo/lysosomal pH) to verify the second-stage pH response. Its zeta potential changed sharply from 11.5 to 42.5 mV within 2 h (Figure 2A) because of the hydrolysis of the lysyl succinyl amides in the ^{SA}TAT moiety and the increased protonation of the amino and guanidinyl groups in K$_{11}$ and TAT.

As we know, the surface property of nanoparticles plays a key role in protein adsorption.[42] Because HSA was used as a model protein, it was found that the MSN-^{SA}TAT&^{DMA}K$_{11}$ nanoparticles can quickly combine with HSA at pH 6.8, and over 58% HSA was adsorbed within 30 min. In addition, the percentage of the adsorbed HSA increased further with a prolonged incubation time (Figure 2B); however, at pH 7.4, MSN-^{SA}TAT&^{DMA}K$_{11}$ nanoparticles showed negligible HSA adsorption even after incubation for 2 h. As the control, MSN-^{SA}TAT&^{SA}K$_{11}$ nanoparticles (all of the amino groups were succinyl amidized) did not interact significantly with protein under the same conditions (Figure 2B). Apparently, the results are consistent with the aforementioned pH-triggered charge-conversional behavior of MSN-^{SA}TAT&^{DMA}K$_{11}$. The zeta potential of MSN-^{SA}TAT&^{DMA}K$_{11}$ became positive gradually, which enhanced the interaction with HSA at pH 6.8, but it remained negative and showed protein resistance at the simulated physiological pH of 7.4. As for MSN-^{SA}TAT&^{SA}K$_{11}$, its zeta potential remained negative, and no charge-conversional behavior could be observed at both pH

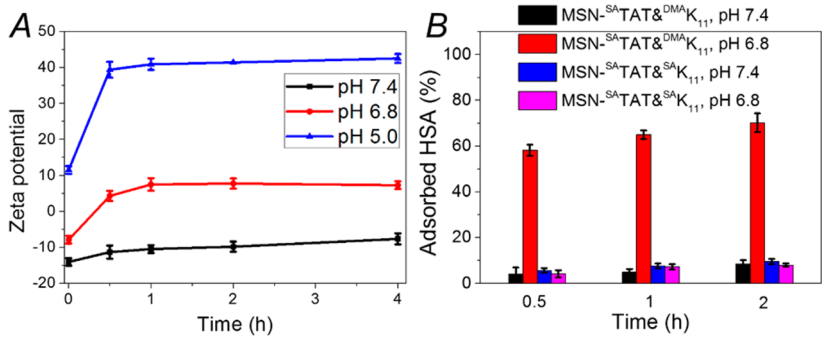

Figure 2. pH-induced zeta potential change of MSN-^{SA}TAT&^{DMA}K$_{11}$ at different pH values (A), and the HSA adsorption on the different nanoparticles after incubation at 37 °C for different periods of time and different pH values (B).

dx.doi.org/10.1021/am503846p | ACS Appl. Mater. Interfaces 2014, 6, 14568−14575

7.4 and 6.8, that is, the nanoparticles showed protein resistance under both physiological and tumoral conditions.

Cellular Uptake Measured by CLSM and Flow Cytometry. It was reported that positively charged nanoparticles are more likely endocytosed by cells than negatively charged ones because of the negatively charged plasma membrane.[24] CLSM was utilized to investigate the uptake behavior of the FITC-MSN-^{SA}TAT&$^{DMA}K_{11}$ nanoparticles at physiological and tumor extracellular pH values. Significantly different cellular uptake behavior was observed for the FITC-MSN-^{SA}TAT&$^{DMA}K_{11}$ nanoparticles at different pH values (Figure 3). At pH 6.8, green spots were found in the cytoplasm

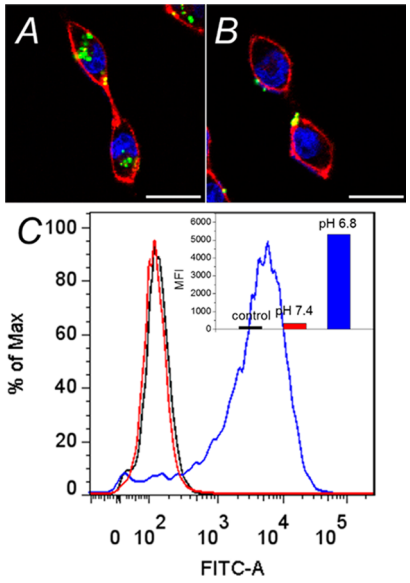

Figure 3. CLSM images of HeLa cells incubated with the FITC-MSN-^{SA}TAT&$^{DMA}K_{11}$ nanoparticles at pH 6.8 (A) and pH 7.4 (B) for 2 h. The plasma membranes and nuclei of the cells were stained with WGA Alexa Fluor 594 conjugate (red) and Hoechst 33342 (blue), respectively. Flow cytometry analysis of HeLa cells treated with the FITC-MSN-^{SA}TAT&$^{DMA}K_{11}$ nanoparticles at pH 6.8 (blue) and pH 7.4 (red) for 2 h (C). Scale bars: 10 μm.

of the HeLa cells, which indicates the internalization by cells, whereas at the physiological pH 7.4, nanoparticles tended to stick on the plasma membrane. FITC-MSN-^{SA}TAT&$^{SA}K_{11}$ was used as the control, and negligible cellular uptake was observed after being incubated with HeLa cells for 2 h at either pH 7.4 or 6.8 (Figure S8, Supporting Information).

Flow cytometry analysis was further utilized to quantitatively evaluate the cellular uptake of different nanoparticles. In accordance with the above results, a remarkable cellular uptake enhancement was found due to the strong intracellular fluorescence at pH 6.8 for FITC-MSN-^{SA}TAT&$^{DMA}K_{11}$ (Figure 3C). Not surprisingly, there was a negligible difference in the intracellular fluorescence between pH 6.8 and 7.4 for the noncharge-conversional FITC-MSN-^{SA}TAT&$^{SA}K_{11}$ nanoparticles (Figure S8C, Supporting Information). Obviously, the charge conversion property facilitates the intracellular internalization of the FITC-MSN-^{SA}TAT&$^{DMA}K_{11}$ nanoparticles, and the $^{DMA}K_{11}$ domain is an irreplaceable moiety for selective cellular uptake.

Nuclear Localization. Fast endo/lysosomal escape is vitally important for the intranuclear localization of the endocytosed MSN-^{SA}TAT&$^{DMA}K_{11}$ nanoparticles. For a better understanding, the FITC-MSN-^{SA}TAT&$^{DMA}K_{11}$ nanoparticles were incubated with HeLa cells for 4 h, and the acidic organelles were stained with Lysotracker Red DND-99. It was found that although some nanoparticles were entrapped in endo/lysosomes as evidenced by the yellow spots (Figure S9C, Supporting Information), many of them were liberated into the cytosol (green dots), which suggests successful escape from the endo/lysosomes. Comparatively, nanoparticles without ^{SA}TAT moiety (FITC-MSN-$^{DMA}K_{11}$) were mainly located in the endo/lysosomes after the same incubation time (data not shown). It was confirmed that the endocytosed nanoparticles could be liberated rapidly into the cytosol from the endo/lysosomes with the facilitation of ^{SA}TAT.

To study the capability of intranuclear import for the endo/lysosomal escaped nanoparticles, FITC-MSN-^{SA}TAT&$^{DMA}K_{11}$ nanoparticles were incubated with HeLa cells. As shown in Figure 4, the cellular uptake increased with time as evidenced

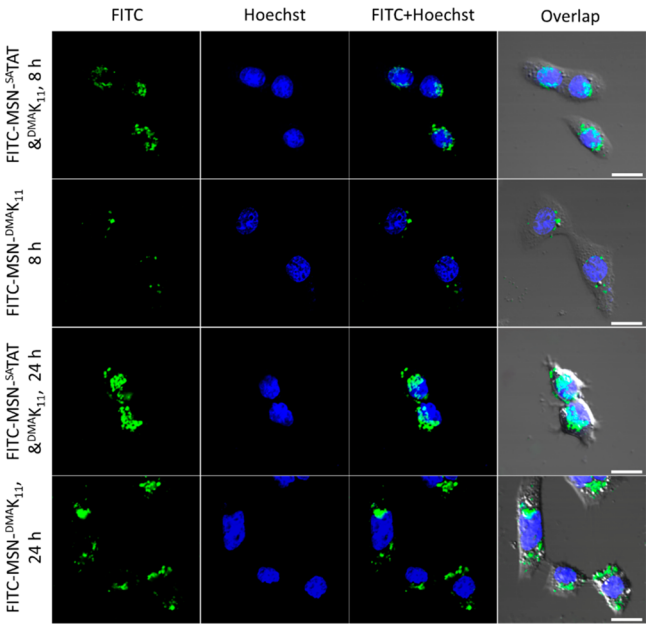

Figure 4. CLSM images of HeLa cells incubated with FITC-MSN-^{SA}TAT&$^{DMA}K_{11}$ or FITC-MSN-$^{DMA}K_{11}$ at pH 6.8 for 8 and 24 h. Scale bars: 20 μm.

by the increased number of green spots. Besides, FITC-MSN-^{SA}TAT&$^{DMA}K_{11}$ nanoparticles were found in both the cytoplasm and nucleoplasm of HeLa cells after incubation for 8 and 24 h, which is further supported by the gallery view of two-color z-stacks (Figure S10, Supporting Information). Meanwhile, the nuclear uptake was found to be increased with time. In contrast, as the control, FITC-MSN-$^{DMA}K_{11}$ nanoparticles were mainly accumulated in the cytoplasm as well as the perinuclear region (Figure 4). A similar phenomenon was observed from the Bio-TEM images after the incubation of HeLa cells with nanoparticles for 24 h. MSN-^{SA}TAT&$^{DMA}K_{11}$ nanoparticles were found in the nucleoplasm (Figure S11A, Supporting Information), while MSN-$^{DMA}K_{11}$ nanoparticles were found in the cytoplasm (Figure S11B, Supporting Information). The existence of silicon in the nucleoplasm was also verified by energy-dispersive X-ray (EDX) analysis (Figure S11C, Supporting Information), which confirms the nuclear localization of the MSN-^{SA}TAT&$^{DMA}K_{11}$ nanoparticles.

In addition, the nuclei were extracted after the incubation of HeLa cells with nanoparticles for 8 and 24 h, and the nuclear uptake of the nanoparticles was silicon-quantified by AAS. The nuclear uptake of MSN-^{SA}TAT&$^{DMA}K_{11}$ was 4.5-fold higher than that of MSN-$^{DMA}K_{11}$ after 8 h of incubation, and the value increased to 10.9-fold after 24 h of incubation (Figure S12, Supporting Information). Apparently, compared to that of MSN-$^{DMA}K_{11}$, the nuclear localization was enhanced significantly with increased time for MSN-^{SA}TAT&$^{DMA}K_{11}$ because of the aid of ^{SA}TAT. Obviously, the hydrolysis of succinyl amides in ^{SA}TAT occurred in the endo/lysosomes, which restored the nucleus-targeting ability of the TAT peptide in FITC-/MSN-^{SA}TAT&$^{DMA}K_{11}$.

To study the intranuclear drug delivery, an anticancer drug DOX was loaded in the pores of MSN-^{SA}TAT&$^{DMA}K_{11}$ and the drug-loading efficiency (DLE) of the nanoparticle was determined by fluorescence spectroscopy. The free DOX, DOX@MSN-^{SA}TAT&$^{DMA}K_{11}$ (DLE = 4.1%), and DOX@MSN-$^{DMA}K_{11}$ (DLE = 3.8%) nanoparticles were separately incubated with HeLa cells at pH 6.8 for 4 h. From Figure 5, it can be found that the cytoplasm and nucleoplasm were filled with red fluorescence for the free DOX because of its diffusion. In the case of DOX@MSN-^{SA}TAT&$^{DMA}K_{11}$, the red fluorescence of the released DOX spread all over the cells, which was similar to what was seen for free DOX. However, for DOX@MSN-$^{DMA}K_{11}$, the red fluorescence was mainly accumulated in the cytoplasm, which implies that DOX cannot be delivered into the nuclei directly by ^{SA}TAT-unconjugated DOX@MSN-$^{DMA}K_{11}$ within 4 h.

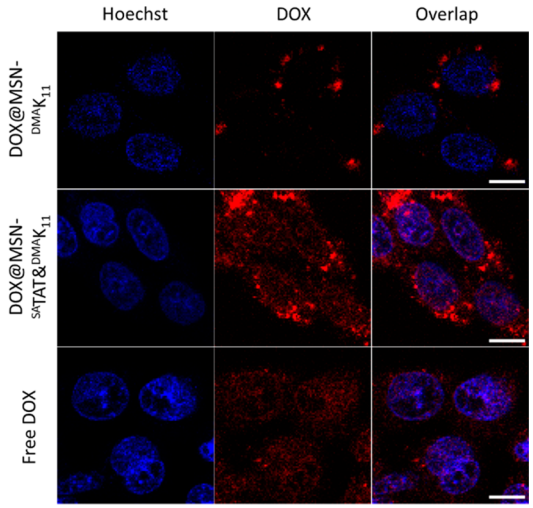

Figure 5. CLSM images for Hela cells incubated with DOX@MSN-$^{DMA}K_{11}$, DOX@MSN-^{SA}TAT&$^{DMA}K_{11}$, and free DOX at pH 6.8 for 4 h. The concentration of DOX was 1 μg mL^{-1}. Scale bars: 10 μm.

The anticancer efficiency of DOX@MSN-^{SA}TAT&$^{DMA}K_{11}$ and DOX@MSN-$^{DMA}K_{11}$ nanoparticles were evaluated in terms of HeLa cells. Before the drug loading, MSN-^{SA}TAT&$^{DMA}K_{11}$ and MSN-$^{DMA}K_{11}$ showed negligible toxicity against HeLa cells with cell viability of over 90% at the concentration of 260 μg mL^{-1} (Figure 6A). After drug loading, compared with DOX@MSN-$^{DMA}K_{11}$, DOX@MSN-^{SA}TAT&$^{DMA}K_{11}$ exhibited much more cytotoxicity (Figure 6B). To seek direct evidence for the enhancement of anticancer efficiency, the DOX uptake in the nucleus was tested after the incubation of DOX@MSN-$^{DMA}K_{11}$ or DOX@MSN-^{SA}TAT&$^{DMA}K_{11}$ with HeLa cells for 8 or 24 h (Figure S14, Supporting Information). It was observed that the nuclear DOX uptake of DOX@MSN-^{SA}TAT&$^{DMA}K_{11}$ was much higher than that of DOX@MSN-$^{DMA}K_{11}$.

CONCLUSIONS

In summary, a novel, intelligent, MSN-based multifunctional MSN-^{SA}TAT&$^{DMA}K_{11}$ was prepared as a stepwise-acid-active DDS for tumor-specific nucleus-targeted drug delivery, which was proved to possess the following features: (i) the nanoparticles maintained a relatively stealthy character with protein and cell resistance under a normal physiological environment; (ii) they transformed into a more cell-interactive form upon arrival at the target tumor site to exhibit promoted cellular uptake via the tumor-acidity-activated charge conversion of dimethylmaleic amides; (iii) fast endo/lysosomal escape occurred with the facilitation of ^{SA}TAT via the hydrolysis of succinyl amides for the internalized nanoparticles; and (iv) the presence of regenerated TAT peptide facilitated the active nuclear import to realize intranuclear drug delivery. We believe the MSN-^{SA}TAT&$^{DMA}K_{11}$ carrier demonstrated here may have a promising potential for cancer therapy.

ASSOCIATED CONTENT

Supporting Information

Synthesis of the peptides; ESI-MS spectra of the peptides; powder X-ray pattern of MSN; FT-IR spectra of MSN, MSN-alkyne, and MSN-^{SA}TAT&$^{DMA}K_{11}$; TGA curves of MSN, MSN-alkyne, and MSN-^{SA}TAT&$^{DMA}K_{11}$; DLS measurements of MSN-^{SA}TAT&$^{DMA}K_{11}$; CLSM, flow cytometry, Bio-TEM, and nuclear uptake analysis of the indicated nanoparticles; and drug release profiles from DOX@MSN-^{SA}TAT&$^{DMA}K_{11}$ at different

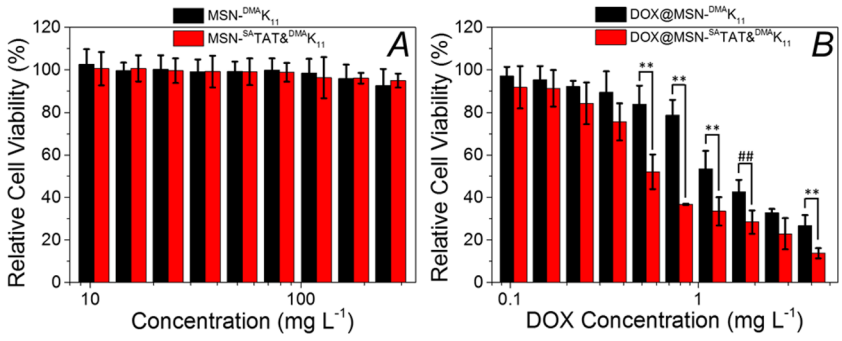

Figure 6. Viability of HeLa cells incubated with nanoparticles before (A) and after (B) DOX loading at different doses. n = 4, data expressed as average ± SE, **denotes p < 0.001, ##denotes p < 0.005.

pH values. This material is available free of charge via the Internet at http://pubs.acs.org.

AUTHOR INFORMATION

Corresponding Author

*E-mail: xz-zhang@whu.edu.cn.

Author Contributions

‡Z.-Y.L. and Y.L. contributed equally to this work.

Notes

The authors declare no competing financial interest.

ACKNOWLEDGMENTS

We acknowledge the financial support from the National Natural Science Foundation of China (51125014 and 51233003), the Ministry of Science and Technology of China (2011CB606202), the Natural Science Foundation of Hubei Province of China (2013CFA003), and the Fundamental Research Fund for the Central Universities (2012203020202).

REFERENCES

(1) Eccles, S. Monoclonal Antibodies Targeting Cancer: "Magic Bullets" or Just the Trigger? *Breast Cancer Res.* **2001**, *3*, 86−90.

(2) Alvisi, G.; Poon, I. K.; Jans, D. A. Tumor-Specific Nuclear Targeting: Promises for Anti-Cancer Therapy? *Drug Resist. Updates* **2006**, *9*, 40−50.

(3) Saha, S.; Leung, K. C. F.; Nguyen, T. D.; Stoddart, J. F.; Zink, J. I. Nanovalves. *Adv. Funct. Mater.* **2007**, *17*, 685−693.

(4) Torney, F.; Trewyn, B. G.; Lin, V. S. Y.; Wang, K. Mesoporous Silica Nanoparticles Deliver DNA and Chemicals into Plants. *Nat. Nanotechnol.* **2007**, *2*, 295−300.

(5) Slowing, I. I.; Vivero-Escoto, J. L.; Wu, C. W.; Lin, V. S. Y. Mesoporous Silica Nanoparticles as Controlled Release Drug Delivery and Gene Transfection Carriers. *Adv. Drug Delivery Rev.* **2008**, *60*, 1278−1288.

(6) Pan, L.; He, Q.; Liu, J.; Chen, Y.; Ma, M.; Zhang, L.; Shi, J. Nuclear-Targeted Drug Delivery of TAT Peptide-Conjugated Monodisperse Mesoporous Silica Nanoparticles. *J. Am. Chem. Soc.* **2012**, *134*, 5722−5725.

(7) Pan, L.; Liu, J.; He, Q.; Wang, L.; Shi, J. Overcoming Multidrug Resistance of Cancer Cells by Direct Intranuclear Drug Delivery Using TAT-Conjugated Mesoporous Silica Nanoparticles. *Biomaterials* **2013**, *34*, 2719−2730.

(8) Wagstaff, K. M.; Jans, D. A. Nuclear Drug Delivery to Target Tumour Cells. *Eur. J. Pharmacol.* **2009**, *625*, 174−180.

(9) Conner, S. D.; Schmid, S. L. Regulated Portals of Entry into the Cell. *Nature* **2003**, *422*, 37−44.

(10) Belting, M.; Sandgren, S.; Wittrup, A. Nuclear Delivery of Macromolecules: Barriers and Carriers. *Adv. Drug Delivery Rev.* **2005**, *57*, 505−527.

(11) Panté, N.; Kann, M. Nuclear Pore Complex Is Able to Transport Macromolecules with Diameters of about 39 nm. *Mol. Biol. Cell* **2002**, *13*, 425−434.

(12) Kubitscheck, U.; Grnwald, D.; Hoekstra, A.; Rohleder, D.; Kues, T.; Siebrasse, J. P.; Peters, R. Nuclear Transport of Single Molecules: Dwell Times at the Nuclear Pore Complex. *J. Cell Biol.* **2005**, *168*, 233−243.

(13) Gerweck, L. E.; Seetharaman, K. Cellular pH Gradient in Tumor versus Normal Tissue: Potential Exploitation for the Treatment of Cancer. *Cancer Res.* **1996**, *56*, 1194−1198.

(14) Egeblad, M.; Werb, Z. New Functions for the Matrix Metalloproteinases in Cancer Progression. *Nat. Rev. Cancer* **2002**, *2*, 161−174.

(15) Du, J. Z.; Sun, T. M.; Song, W. J.; Wu, J.; Wang, J. A. A Tumor-Acidity-Activated Charge-Conversional Nanogel as an Intelligent Vehicle for Promoted Tumoral-Cell Uptake and Drug Delivery. *Angew. Chem., Int. Ed.* **2010**, *49*, 3621−3626.

(16) Quan, C. Y.; Chen, J. X.; Wang, H. Y.; Li, C.; Chang, C.; Zhang, X. Z.; Zhuo, R. X. Core−Shell Nanosized Assemblies Mediated by the Alpha−Beta Cyclodextrin Dimer with a Tumor-Triggered Targeting Property. *ACS Nano* **2010**, *4*, 4211−4219.

(17) Zhang, J.; Yuan, Z. F.; Wang, Y.; Chen, W. H.; Luo, G. F.; Cheng, S. X.; Zhuo, R. X.; Zhang, X. Z. Multifunctional Envelope-Type Mesoporous Silica Nanoparticles for Tumor-Triggered Targeting Drug Delivery. *J. Am. Chem. Soc.* **2013**, *135*, 5068−5073.

(18) Mok, H.; Veiseh, O.; Fang, C.; Kievit, F. M.; Wang, F. Y.; Park, J. O.; Zhang, M. pH-Sensitive siRNA Nanovector for Targeted Gene Silencing and Cytotoxic Effect in Cancer Cells. *Mol. Pharmaceutics* **2010**, *7*, 1930−1939.

(19) Padilla-Parra, S.; Matos, P. M.; Kondo, N.; Marin, M.; Santos, N. C.; Melikyan, G. B. Quantitative Imaging of Endosome Acidification and Single Retrovirus Fusion with Distinct Pools of Early Endosomes. *Proc. Natl. Acad. Sci. U. S. A.* **2012**, *109*, 17627−17632.

(20) Zhou, Z. X.; Shen, Y. Q.; Tang, J. B.; Fan, M. H.; Van Kirk, E. A.; Murdoch, W. J.; Radosz, M. Charge-Reversal Drug Conjugate for Targeted Cancer Cell Nuclear Drug Delivery. *Adv. Funct. Mater.* **2009**, *19*, 3580−3589.

(21) Du, J. Z.; Du, X. J.; Mao, C. Q.; Wang, J. Tailor-Made Dual pH-Sensitive Polymer-Doxorubicin Nanoparticles for Efficient Anticancer Drug Delivery. *J. Am. Chem. Soc.* **2011**, *133*, 17560−17563.

(22) Lee, Y.; Miyata, K.; Oba, M.; Ishii, T.; Fukushima, S.; Han, M.; Koyama, H.; Nishiyama, N.; Kataoka, K. Charge-Conversion Ternary Polyplex with Endosome Disruption Moiety: A Technique for Efficient and Safe Gene Delivery. *Angew. Chem., Int. Ed.* **2008**, *47*, 5163−5166.

(23) Gratton, S. E.; Ropp, P. A.; Pohlhaus, P. D.; Luft, J. C.; Madden, V. J.; Napier, M. E.; DeSimone, J. M. The Effect of Particle Design on Cellular Internalization Pathways. *Proc. Natl. Acad. Sci. U. S. A.* **2008**, *105*, 11613−11618.

(24) Cho, E. C.; Xie, J.; Wurm, P. A.; Xia, Y. Understanding the Role of Surface Charges in Cellular Adsorption versus Internalization by Selectively Removing Gold Nanoparticles on the Cell Surface with a I2/KI Etchant. *Nano Lett.* **2009**, *9*, 1080−1084.

(25) Lee, Y.; Fukushima, S.; Bae, Y.; Hiki, S.; Ishii, T.; Kataoka, K. A Protein Nanocarrier from Charge-Conversion Polymer In Response to Endosomal pH. *J. Am. Chem. Soc.* **2007**, *129*, 5362−5363.

(26) Lai, C. Y.; Wiethoff, C. M.; Kickhoefer, V. A.; Rome, L. H.; Nemerow, G. R. Vault Nanoparticles Containing an Adenovirus-Derived Membrane Lytic Protein Facilitate Toxin and Gene Transfer. *ACS Nano* **2009**, *3*, 691−699.

(27) Kelly, C. V.; Liroff, M. G.; Triplett, L. D.; Leroueil, P. R.; Mullen, D. G.; Wallace, J. M.; Meshinchi, S.; Baker, J. R.; Orr, B. G.; Banaszak Holl, M. M. Stoichiometry and Structure of Poly(amidoamine) Dendrimer-Lipid Complexes. *ACS Nano* **2009**, *3*, 1886−1896.

(28) Obata, Y.; Tajima, S.; Takeoka, S. Evaluation of pH-Responsive Liposomes Containing Amino Acid-Based Zwitterionic Lipids for Improving Intracellular Drug Delivery in Vitro and in Vivo. *J. Controlled Release* **2010**, *142*, 267−276.

(29) Lee, E. S.; Kim, D.; Youn, Y. S.; Oh, K. T.; Bae, Y. H. A Virus-Mimetic Nanogel Vehicle. *Angew. Chem., Int. Ed.* **2008**, *47*, 2418−2421.

(30) Ke, C. J.; Su, T. Y.; Chen, H. L.; Chiang, H. L.; Chu, P. C.; Xia, Y.; Sung, H. W. Smart Multifunctional Hollow Microspheres for the Quick Release of Drugs in Intracellular Lysosomal Compartments. *Angew. Chem., Int. Ed.* **2011**, *50*, 8086−8089.

(31) You, J. O.; Auguste, D. T. Nanocarrier Cross-Linking Density and pH Sensitivity Regulate Intracellular Gene Transfer. *Nano Lett.* **2009**, *9*, 4467−4473.

(32) Yu, H.; Zou, Y.; Wang, Y.; Huang, X.; Huang, G.; Sumer, B. D.; Boothman, D. A.; Gao, J. Overcoming Endosomal Barrier by Amphotericin B-Loaded Dual pH-Responsive PDMA-*b*-PDPA Micelleplexes for siRNA Delivery. *ACS Nano* **2011**, *5*, 9246−9255.

(33) Endoh, T.; Ohtsuki, T. Cellular siRNA Delivery Using Cell-Penetrating Peptides Modified for Endosomal Escape. *Adv. Drug Delivery Rev.* **2009**, *61*, 704−709.

(34) Nakielny, S.; Dreyfuss, G. Transport of Proteins and RNAs in and out of the Nucleus. *Cell* **1999**, *99*, 677−690.
(35) Patel, S. S.; Belmont, B. J.; Sante, J. M.; Rexach, M. F. Natively Unfolded Nucleoporins Gate Protein Diffusion across the Nuclear Pore Complex. *Cell* **2007**, *129*, 83−96.
(36) Alber, F.; Dokudovskaya, S.; Veenhoff, L. M.; Zhang, W.; Kipper, J.; Devos, D.; Suprapto, A.; Karni-Schmidt, O.; Williams, R.; Chait, B. T. The Molecular Architecture of the Nuclear Pore Complex. *Nature* **2007**, *450*, 695−701.
(37) Jin, E.; Zhang, B.; Sun, X.; Zhou, Z.; Ma, X.; Sun, Q.; Tang, J.; Shen, Y.; Van Kirk, E. A.; Murdoch, W. J.; Radosz, M. Acid-Active Cell-Penetrating Peptides for In Vivo Tumor-Targeted Drug Delivery. *J. Am. Chem. Soc.* **2013**, *135*, 933−940.
(38) Rong, L.; Liu, L. H.; Chen, S.; Cheng, H.; Chen, C. S.; Li, Z. Y.; Qin, S. Y.; Zhang, X. Z. A Coumarin Derivative as a Fluorogenic Glycoproteomic Probe for Biological Imaging. *Chem. Commun.* **2014**, *50*, 667−669.
(39) Suzuki, K.; Ikari, K.; Imai, H. Synthesis of Silica Nanoparticles Having a Well-Ordered Mesostructure Using a Double Surfactant System. *J. Am. Chem. Soc.* **2004**, *126*, 462−463.
(40) Patil, S.; Sandberg, A.; Heckert, E.; Self, W.; Seal, S. Protein Adsorption and Cellular Uptake of Cerium Oxide Nanoparticles as a Function of Zeta Potential. *Biomaterials* **2007**, *28*, 4600−4607.
(41) Amblard, M.; Fehrentz, J. A.; Martinez, J.; Subra, G. Methods and Protocols of Modern Solid Phase Peptide Synthesis. *Mol. Biotechnol.* **2006**, *33*, 239−254.
(42) Sigal, G. B.; Mrksich, M.; Whitesides, G. M. Effect of Surface Wettability on the Adsorption of Proteins and Detergents. *J. Am. Chem. Soc.* **1998**, *120*, 3464−3473.